YTHDC2 serves a distinct late role in spermatocytes during germ cell differentiation

Alexis S. Bailey[1] and Margaret T. Fuller[1*]

[1]Department of Developmental Biology, Stanford University School of Medicine, Stanford, CA, 94305, USA

[*] Corresponding author, lead contact for the manuscript.

Email address: mtfuller@stanford.edu

ORC ID: 0000-0002-3804-4987

ABSTRACT

Post-transcriptional regulation of gene expression by RNA-binding proteins helps facilitate fast, clean transitions from one cell state to the next during germ cell differentiation. Previously we showed that the RNA helicase YTHDC2 is required for germ cells to properly switch from mitosis to meiosis (Bailey et al., 2017). While YTHDC2 protein is first expressed as male germ cells enter meiosis, when it is needed to shut down the mitotic program, YTHDC2 expression continues to increase and reaches its highest levels later in meiotic prophase, in pachytene spermatocytes. Here we show that YTHDC2 has an additional essential role regulating meiotic progression in late spermatocytes during mouse germ cell differentiation. Inducing conditional knockout of *Ythdc2* during the first wave of spermatogenesis, after the germ cells have already initiated meiotic prophase, allowed *Ythdc2*-deficient germ cells to successfully reach the pachytene stage and properly express many meiotic markers. However, instead of continuing through meiotic prophase and initiating the meiotic divisions, late pachytene spermatocytes failed to transition to the diplotene stage and quickly died. Loss of function of *Ythdc2* in spermatocytes resulted in changes in transcript levels for a number of genes, some up-regulated and some down-regulated, compared to control mid-stage spermatocytes. YTHDC2 interacts with different proteins in early and late spermatocytes, with many of the interacting proteins involved in post-transcriptional RNA regulation and present in RNA granules, similar to YTHDC2. Our findings suggest that YTHDC2 facilitates proper progression of germ cells through multiple steps of meiosis, potentially via several mechanisms of post-transcriptional RNA regulation.

33 **INTRODUCTION**

34 RNA-binding proteins and post-transcriptional regulation of RNAs play fundamental
35 roles in germ cell development, allowing a properly timed transition from the mitotic to the
36 meiotic program and clean progression of germ cells through meiotic prophase and terminal
37 differentiation. The DExH-box RNA helicase, YTHDC2, is the mammalian homolog of
38 *Drosophila* Benign gonial cell neoplasm (Bgcn), which along with its protein binding partners
39 Bag of marbles (Bam) and Tumorous testis (Tut), regulate the switch from mitotic divisions to
40 meiosis in males through direct interaction with the 3′UTR of RNAs in the *Drosophila* germline
41 (Chen et al., 2014; Insco et al., 2012). Previous studies from our lab and others have shown that
42 YTHDC2 is first expressed in early spermatocytes, and is required to properly execute the
43 transition from mitosis to meiosis in the mouse germline (Bailey et al., 2017; Hsu et al., 2017;
44 Jain et al., 2018; Liu et al., 2021; Wojtas et al., 2017). *Ythdc2* null mutant germ cells enter
45 meiotic prophase and start to express some meiotic factors, but fail to down-regulate certain
46 mitotic regulators and have a mixed identity (Bailey et al., 2017; Li et al., 2022). Meiotic germ
47 cells in *Ythdc2* null mutants attempt an aberrant mitosis-like metaphase then quickly die by
48 apoptosis. As YTHDC2 localizes to the cytoplasm and has been shown to directly bind specific
49 RNA transcripts, including the mitotic cyclin *Ccna2* (Bailey et al., 2017; Saito et al., 2022),
50 YTHDC2 likely regulates gene expression post-transcriptionally, similar to *Drosophila Bgcn*.

51 YTHDC2 protein contains two ankyrin (ANK) repeats, which typically mediate protein-
52 protein interactions (Li et al., 2006). Previous studies have shown that YTHDC2 binds the
53 meiotic protein MEIOC (Abby et al., 2016; Bailey et al., 2017; Li et al., 2022; Soh et al., 2017)
54 as well as the RNA-binding protein RBM46 (Li et al., 2022; Qian et al., 2022). Binding of
55 YTHDC2 to both MEIOC and RBM46 does not require RNA. *Meioc* and *Rbm46* knockout males

56 show the same early spermatocyte death phenotype as *Ythdc2* null mutants (Abby et al., 2016;
57 Peart et al., 2022; Qian et al., 2022; Soh et al., 2017), suggesting that YTHDC2, MEIOC and
58 RBM46 function together to regulate the switch from mitosis to meiosis in males. Directly tying
59 YTHDC2 target RNAs to degradation machinery and supporting a functional role for YTHDC2
60 in regulating RNA stability, previous studies have also shown that the cytoplasmic 5′ → 3′
61 exoribonuclease XRN1 is a direct, RNA-independent binding partner of YTHDC2, interacting
62 via the YTHDC2 ANK domain (Kretschmer et al., 2018; Li et al., 2022; Wojtas et al., 2017).
63 While YTHDC2 protein expression starts as male germ cells enter meiosis, western blot
64 analysis indicated that YTHDC2 protein levels increase during the first wave of spermatogenesis
65 as germ cells proceed through meiotic prophase (Bailey et al., 2017). As *Ythdc2* null mutant
66 germ cells die very soon after entry into meiotic prophase, it was not possible to investigate
67 whether YTHDC2 plays important roles in male germ cell differentiation after its role in shutting
68 down the mitotic program. Also, the abnormally low levels of many meiotic RNAs such as
69 *Spo11*, observed in testes from *Ythdc2* null mutant males, could be a secondary effect of the
70 death of young spermatocytes early in meiotic prophase. Here we examine the effects of loss of
71 function of *Ythdc2* in later spermatocytes to shed light on another molecular role of this pivotal
72 protein in germ cell development.
73 Our results show that in addition to its role in the mitosis-to-meiosis transition, YTHDC2
74 has another critical role in promoting progression of spermatocytes through late meiotic
75 prophase. To carefully study the direct consequences of *Ythdc2* loss of function in late meiotic
76 prophase, we induced conditional knockout of *Ythdc2* at a specific stage during the first wave of
77 spermatogenesis. This strategy allowed us to largely bypass the early mitosis-to-meiosis defects
78 previously observed in *Ythdc2* null mutants. Induced deletion of *Ythdc2* in early spermatocytes

79 allowed the germ cells to properly progress to the pachytene stage and express meiotic markers.
80 However, changes in gene expression were apparent in pachytene stage spermatocytes three days
81 post tamoxifen, followed by elimination of late pachytene spermatocytes by apoptosis prior to
82 the meiotic divisions. Immunoprecipitation experiments revealed that YTHDC2 protein interacts
83 with several RNA-binding proteins with roles in mRNA metabolism in early and late
84 spermatocytes, supporting the idea that YTHDC2 functions at multiple stages of germ cell
85 development to facilitate proper entry and execution of meiosis.

86 **RESULTS**

87 **YTHDC2 is highly expressed in late spermatocytes.**

88 Immunofluorescence staining detected YTHDC2 protein starting in early spermatocytes,
89 with expression continuing throughout meiotic prophase, as previously reported (Bailey et al.,
90 2017; Jain et al., 2018). Similar immunofluorescence staining of cross-sections of testis tubules
91 from males 18 days after birth (P18) showed low levels of YTHDC2 signal in the cytoplasm of
92 early leptotene spermatocytes (Figure 1A, white arrowheads) and high levels of cytoplasmic
93 YTHDC2 signal in the late pachytene spermatocytes that occupy the center of the testis tubules
94 (Figure 1A, white arrows), raising the question of whether YTHDC2 has a critical function in
95 late spermatocytes in addition to its role in early meiotic prophase.

96 To bypass the early *Ythdc2* null mutant phenotype and examine the function of YTHDC2
97 in late meiotic prophase, we generated mice bearing a conditional *Ythdc2* allele (*Ythdc2*^{flox})
98 (Figure 1-figure supplement 1) with *loxP* sites flanking exons 6 and 7. *Ythdc2*^{flox} mice were
99 crossed to our previously generated mice carrying the *Ythdc2* null allele (*Ythdc2*$^{\Delta}$) (Bailey et al.,
100 2017). We then introduced the tamoxifen-inducible transgene *UBC-Cre-ERT2* (Ruzankina et al.,

101 2007), which expresses Cre-ERT2 under the control of the ubiquitin C (UBC) promoter.
102 Treatment of *UBC-Cre-ERT2; Ythdc2*$^{flox/\Delta}$ (*Ythdc2* cKO) juvenile mice with tamoxifen at P12
103 and P13, when the first wave of germ cells have already entered meiotic prophase and are in the
104 leptotene/zygotene stage (Figure 1B), allowed expression of YTHDC2 protein in early-stage
105 spermatocytes but substantially reduced levels of YTHDC2 protein expression in late-stage
106 spermatocytes. YTHDC2 protein was expressed at similar levels in control and *UBC-Cre-ERT2;*
107 *Ythdc2*$^{flox/\Delta}$ early spermatocytes at P12, the time of the first tamoxifen injection (Figure 1C,D).
108 Immunofluorescence staining showed that YTHDC2 protein levels started to decrease by just
109 one day after the second tamoxifen injection (P14) in *Ythdc2* cKO tubules compared to controls
110 (Figure 1F vs. E), although low levels of YTHDC2 protein were still detected in approximately
111 50% of the *Ythdc2* cKO tubules (Figure 1O). By P16, while control spermatocytes continued to
112 have high levels of YTHDC2 protein expression (Figure 1G), the level of YTHDC2 protein in
113 spermatocytes detected by immunofluorescence staining was considerably lower in *Ythdc2* cKO
114 testis tubules (Figure 1H). Quantification of the percentage of tubules that contained YTHDC2-
115 positive spermatocytes confirmed that YTHDC2 protein expression was below the level of
116 detection by our immunofluorescence staining in the majority of *Ythdc2* cKO testis tubules by
117 P16 (Figure 1O).

118 **YTHDC2 is required for late spermatocytes to progress through meiotic prophase.**

119 Analysis of testis tubule cross-sections from the *Ythdc2* cKO males showed that the
120 timing of the tamoxifen treatment allowed male germ cells to proceed past the initial requirement
121 for YTHDC2 function early in meiotic prophase. Our previous studies revealed that in *Ythdc2*
122 null mutant mice, a large number of germ cells underwent abnormal chromosome condensation
123 soon after initiating meiotic prophase (Bailey et al., 2017), visible as abnormal metaphase-like

124 spermatocytes in P12 testes. This phenotype was also observed in *Meioc* and *Rbm46* knockout
125 males (Abby et al., 2016; Qian et al., 2022; Soh et al., 2017). Quantification of testis tubule
126 cross-sections revealed that only a small percentage of tubules in *Ythdc2* cKO mice contained
127 cells with condensed chromosomes. This observation was made at both P16 (control 1.4% vs.
128 *Ythdc2* cKO 8.7%) and P18 (control 0% vs. *Ythdc2* cKO 3.9%). Consistent with the small
129 number of cells with abnormal chromosomal condensation in *Ythdc2* cKO mice, *Ythdc2* cKO
130 spermatocytes did not express the abnormal high levels of CYCLINA2 in spermatocytes
131 previously observed in P12 *Ythdc2* null mutant males (Figure 1Q,S vs. P), indicating that
132 inducing knockout of *Ythdc2* starting at P12 allowed the majority of germ cells to get past the
133 requirement to shut down the mitotic program during the first wave of spermatogenesis.
134 Examination of histological sections of P16 testes showed that unlike *Ythdc2* null mutant germ
135 cells, which never reached the pachytene spermatocyte stage (Bailey et al., 2017), *Ythdc2* cKO
136 germ cells moved successfully through the early spermatocyte stages and reached the pachytene
137 stage at a similar frequency to controls (Figure 2E,F and M). By P20, while control tubules were
138 filled with late-stage spermatocytes (Figure 2I), the majority of tubules in *Ythdc2* cKO mice
139 lacked late spermatocytes (Figure 2J). *Ythdc2* cKO tubules were empty of all spermatocyte
140 stages by P25 (Figure 2L).

141 Immunofluorescence staining revealed that *Ythdc2* cKO pachytene spermatocytes express
142 and localize meiotic markers similar to control spermatocytes. At P16, *Ythdc2* cKO tubules were
143 filled with pachytene spermatocytes that express high levels of the synaptonemal complex
144 component SYCP3 (Figure 3A,B). Analysis of germ cell spreads revealed that SYCP3 properly
145 localized on the chromosome axis in early (Figure 3E-H) and late (Figure 3I,J) spermatocytes
146 from *Ythdc2* cKO males as in controls. *Ythdc2* cKO early prophase spermatocytes appeared to

147 properly make double strand breaks (DSBs), as immunofluorescence staining of chromosome
148 spreads showed γH2AX foci along the chromosomes in leptotene (Figure 3E,F) and zygotene
149 (Figure 3G,H) spermatocytes. In pachytene spermatocytes, γH2AX became restricted to the sex
150 vesicle containing the X and Y chromosomes in *Ythdc2* cKO males, similar to the control (Figure
151 3I,J). Analysis of the dynamics of RAD51 expression in chromosome spreads revealed that
152 RAD51 foci were present at the zygotene stage (Figure 3-figure supplement 1A,B) then
153 decreased in number in *Ythdc2* cKO pachytene spermatocytes similar to control (Figure 3-figure
154 supplement 1C-F), suggesting that the double strand breaks were being properly repaired.
155 While pachytene spermatocytes appeared to have normal morphology and properly
156 express meiotic markers at P16, the *Ythdc2* cKO germ cells failed to advance past the late
157 pachytene stage and quickly underwent apoptosis, suggesting that YTHDC2 is required for late
158 spermatocytes to complete meiotic prophase. Analysis of tubule cross-sections and cell spreads
159 showed that while control tubules contained diplotene spermatocytes by P18 (Figure 2M and
160 3K), *Ythdc2* cKO male germ cells progressed to the diplotene stage very rarely (one diplotene
161 cell in > 500 tubule cross-sections). Rather, primarily late pachytene spermatocytes were present
162 in the P18 *Ythdc2* cKO tubules (Figure 2M and 3L). TUNEL staining showed a slight increase in
163 the number of TUNEL-positive cells in *Ythdc2* cKO testes compared to controls starting at P16
164 (Figure 3N vs. M, quantified in Q). However, the number of TUNEL-positive cells per tubule
165 cross-section greatly increased at P18 in *Ythdc2* cKO tubules compared to controls (Figure 3P vs.
166 O, quantified in Q), with some tubules filled with TUNEL-positive spermatocytes in the *Ythdc2*
167 cKO (Figure 3P, white arrow).
168 In addition to the inducible *Ythdc2* knockout model, $Ythdc2^{flox/\Delta}$ conditional mice were
169 also crossed to mice carrying the *Spo11-Cre* transgene, which expresses CRE recombinase in

170 spermatocytes that have initiated meiosis (Lyndaker et al., 2013). Consistent with the findings
171 from the inducible *UBC-Cre-ERT2; Ythdc2*$^{flox/\Delta}$ mice, examination of P18 control and *Spo11-*
172 *Cre; Ythdc2*$^{flox/\Delta}$ testis tubules revealed that YTHDC2 was required to complete meiotic
173 prophase. *Spo11-Cre; Ythdc2*$^{flox/\Delta}$ germ cells reached the pachytene stage of meiotic prophase, as
174 scored by immunofluorescence staining for γH2AX, which was restricted to the sex body as in
175 control pachytene spermatocytes (Figure 3-figure supplement 2C,D). However, the
176 spermatocytes then quickly started to die, leading to some tubules lacking late spermatocytes in
177 P18 *Spo11-Cre; Ythdc2*$^{flox/\Delta}$ testes (Figure 3-figure supplement 2B). Furthermore, analysis of
178 histological sections from adult testis revealed that while the *Spo11-Cre; Ythdc2*$^{flox/\Delta}$ model was
179 not as penetrant as the inducible system, a large proportion of tubules lacked late-stage germ
180 cells (Figure 3-figure supplement 2F vs. E), and mature sperm were rarely seen in cross-sections
181 of the epididymis (Figure 3-figure supplement 2H vs. G). Taken together, our data from analysis
182 of both the cell-stage specific and the inducible *Ythdc2* knockout mice revealed that in addition
183 to its early role at the mitotic-to-meiotic transition, YTHDC2 has a distinct, later role in meiotic
184 prophase regulating the pachytene-to-diplotene transition.

185 **YTHDC2 interacts with several other proteins involved in RNA regulation.**

186 Consistent with its role in RNA regulation, YTHDC2 appears to interact with several
187 other proteins involved in RNA biology, including RNA stability, RNA localization and
188 translation. Immunoprecipitation of YTHDC2 from P12 and P18 wild-type testes followed by
189 mass spectrometry revealed several novel candidate protein interacting partners for YTHDC2.
190 As YTHDC2 is an RNA-binding protein, we validated candidate interacting partners by
191 performing co-immunoprecipitation experiments in the presence and absence of RNase to
192 uncover which proteins interact with YTHDC2 independently of RNA. Multiple proteins co-

193 immunoprecipitated with YTHDC2 from RNase-treated testis extracts including the previously
194 known interacting protein MEIOC as well as several additional proteins, including PABPC1,
195 FMR1, CAPRIN1, PTBP1 and EWS (Figure 4A). MEIOC, PABPC1 and FMR1 showed
196 particularly strong binding to YTHDC2 at P18 independent of RNA, while the hnRNP PTBP1
197 appeared to co-immunoprecipitate with YTHDC2 at low levels in the presence of RNase at P12.
198 In addition to RNA-independent protein interactors, we identified three additional proteins that
199 immunoprecipitated with YTHDC2 only in the presence of RNA, including MOV10, YBX1,
200 G3BP2 and UPF1 (Figure 4B). Immunofluorescence staining of YTHDC2 and the protein
201 binding partners in wild-type testes showed that the interactors were all highly expressed in the
202 cytoplasm at specific spermatocyte stages. Some of the interactors were expressed at high levels
203 primarily in early leptotene and zygotene spermatocytes, including PTBP1, MOV10 and G3BP2,
204 while other interactors were highly expressed in pachytene spermatocytes, including PABPC1,
205 CAPRIN1, YBX1 and UPF1 (Table 1).
206 MEIOC protein strongly co-immunoprecipitated with YTHDC2 from both P12 and P18
207 testes in the absence of RNA. Immunofluorescence staining of MEIOC and SYCP3 in P18 testes
208 revealed that control and *Ythdc2* cKO tubules contained both pachytene spermatocytes (Figure
209 4C′ and F′, box 1) as well as leptotene spermatocytes from the second wave of spermatogenesis
210 (Figure 4C′ and F′, box 2). In control testes, MEIOC was expressed in both pachytene (Figure
211 4D) and leptotene (Figure 4E) spermatocytes as previously shown (Abby et al., 2016; Soh et al.,
212 2017). However, while MEIOC was present in the P18 *Ythdc2* cKO pachytene spermatocytes
213 (Figure 4G), MEIOC was not detected by immunofluorescence in the *Ythdc2* cKO leptotene
214 spermatocytes from the second wave (Figure 4H), suggesting YTHDC2 may promote the
215 stability of MEIOC in early spermatocytes.

216 While MEIOC protein was present throughout the cytoplasm of *Ythdc2* cKO
217 spermatocytes, it also appeared to concentrate in perinuclear puncta (Figure 4G, white arrows).
218 In control spermatocytes, MEIOC protein was highly expressed throughout the cytoplasm and
219 did not appear to accumulate as strongly in perinuclear puncta (Figure 4D). We have previously
220 shown that YTHDC2 protein localizes to RNA granules in spermatocytes (Bailey et al., 2017).
221 Co-staining with antibodies against two RNA granule components, the decapping enzyme
222 DCP1A and the mouse PIWI family protein MIWI, revealed that many of the MEIOC-positive
223 cytoplasmic puncta present in *Ythdc2* cKO spermatocytes also contained DCP1A and MIWI
224 (Figure 4I-I′′′, white arrows).

225 **Early transcript changes following knockout of *Ythdc2* in spermatocytes.**

226 Comparison of RNA expression in *Ythdc2* cKO and control testes by RNA sequencing
227 revealed very early changes in gene expression upon conditional knockout of *Ythdc2* in late
228 spermatocytes. To observe early changes in gene expression following *Ythdc2* knockout that
229 occur before the germ cells begin to die, we performed bulk RNA sequencing from control and
230 *Ythdc2* cKO testes at P14 and P16 following two days of tamoxifen injections at P12 and P13.
231 Principle component analysis (PCA) revealed that RNA expression in testes from control and
232 *Ythdc2* cKO mice were similar at P14 (Figure 5A). At this time point, only one day post the
233 second tamoxifen injection, levels of YTHDC2 protein detected by immunofluorescence staining
234 of testis tubules were decreasing but YTHDC2 protein was still detected in some tubules (Figure
235 1F and 1O). While *Ythdc2* RNA expression was significantly down-regulated in the *Ythdc2* cKO
236 testes compared to controls at P14, there were only five other mRNAs that showed significant
237 changes in expression between control and *Ythdc2* cKO testes (*Aqp1*, *Lars2*, *Hbb-b1*, *Ndor1* and
238 *Meioc*) (Figure 5B). At P16, the *Ythdc2* cKO replicates clustered, and the control P16 replicates

239 clustered with each other but the two genotypes were widely separated in gene expression space
240 (Figure 5A).
241 Many RNAs were significantly different at P16 in the *Ythdc2* cKO testes compared to
242 controls (Figure 5C). Further examination of the significant differentially expressed transcripts in
243 P16 *Ythdc2* cKO testes compared to controls ($p < 0.05$, Log2FC ≥ 1 or ≤ -1, 294 total genes)
244 (Figure 5 – source data 1) revealed that nearly half (129/294) of the differentially expressed
245 RNAs were up-regulated in the *Ythdc2* cKO testes compared to controls (Figure 5D). GO-term
246 analysis of the 129 RNAs up-regulated in *Ythdc2* cKO P16 testes compared to controls showed
247 enrichment for RNAs associated with viral response and response to interferon-beta, consistent
248 with the initiation of programed cell death characteristic of late spermatocytes in the *Ythdc2*
249 cKO. Interestingly, we observed a much larger number of RNAs up-regulated in the conditional
250 *Ythdc2* knockout (n = 129 up-regulated genes) compared to the number of RNAs up-regulated in
251 the P12 *Ythdc2* null mutant RNA-seq dataset (n = 19 up-regulated genes) (Bailey et al., 2017),
252 suggesting that YTHDC2 may act in mid to late spermatocytes to target a number of RNAs for
253 degradation.
254 In addition, 165 RNAs were down-regulated in P16 *Ythdc2* cKO testes compared to
255 controls. GO-term analysis revealed that the most down-regulated RNAs in *Ythdc2* cKO versus
256 controls were enriched for RNAs associated with chromatin assembly/organization and meiosis
257 (Figure 5E). Consistent with immunofluorescence experiments revealing proper protein
258 expression of the meiotic markers SYCP3, γH2AX and RAD51 in P16 *Ythdc2* cKO
259 spermatocytes, expression of many meiotic transcripts was not significantly affected in P16
260 *Ythdc2* cKO mice compared to controls. However, there was a subset of meiotic transcripts

261 (*Rec114*, *M1ap*, *Msh5*, *Prdm9*, *Zcwpw1*, *Mei4*, *Ccnb1ip1*, *Stra8*, *Rad21l* and *Mei1*) that were
262 significantly down-regulated in *Ythdc2* cKO testes compared to controls.

263 Comparison of our RNA-seq data at P16 to two recently published CLIP-seq datasets
264 from P15 testes (Li et al., 2022) and adult testes (Saito et al., 2022) revealed that many of the top
265 transcripts differentially expressed in *Ythdc2* cKO testes compared to controls were directly
266 bound by YTHDC2 (Figure 5 – source data 1). Overall, only 21% of the 249 differentially
267 expressed transcripts were identified as YTHDC2 targets in either CLIP-seq dataset. However,
268 further analysis revealed that 76% of the top 25 most significant differentially expressed
269 transcripts were YTHDC2 targets, suggesting that the expression changes may be a direct
270 consequence of *Ythdc2* knockout since YTHDC2 binds these transcripts. Some of the top
271 transcripts present at higher levels in P16 *Ythdc2* cKO testes were directly bound by YTHDC2,
272 including *Meioc* RNA, suggesting that the YTHDC2/MEIOC protein binding complex may help
273 regulate their own levels of expression. In addition, many of the top transcripts present at lower
274 levels in *Ythdc2* cKO testes were also directly bound by YTHDC2, including many of the highly
275 down-regulated histones (*H4c11*, *H4c12*, *H2bc14* and *H2bu2*) (Figure 5C), suggesting that
276 YTHDC2 may stabilize these RNAs.

277 **DISCUSSION**

278 The RNA-binding protein YTHDC2 plays two distinct roles in early versus late meiotic
279 prophase. Germ cells in *Ythdc2* null mutant testes attempt to enter meiosis but fail to properly
280 shut down the mitotic program, leading to an abnormal, mitosis-like division and apoptosis. Here
281 we show that YTHDC2 has a second, critical role in pachytene spermatocytes, where it is
282 required for meiotic progression during the late pachytene stage. Upon conditional knockout of
283 *Ythdc2* in early spermatocytes at P12 during the first wave of spermatogenesis, germs cells

284 properly expressed and localized multiple meiotic markers and, unlike *Ythdc2* null mutant
285 leptotene spermatocytes, they did not express CYCLINA2 or undergo abnormal chromatin
286 condensation, indicating that the cells committed to meiosis and successfully progressed to the
287 pachytene stage. However, changes in gene expression were quickly observed by P16, and the
288 *Ythdc2* cKO spermatocytes failed to complete the pachytene-to-diplotene transition and instead
289 underwent apoptosis.

290 Because we induced *Ythdc2* knockout at P12 and P13 during the first wave of
291 spermatogenesis and analyzed testes starting one day post two tamoxifen injections, our
292 experimental setup did not have later germ cell stages, allowing us to clearly observe the initial
293 defects that occur upon knockout of *Ythdc2* as the germ cells proceed synchronously through
294 meiotic prophase. Our studies agree with observations made by Liu and colleagues, who
295 analyzed the effects of conditional knockout of *Ythdc2* in adult testis (Liu et al., 2021), but our
296 studies are more focused on the initial, likely more direct effects of loss of YTHDC2 function in
297 spermatocytes. Because adult testes have germ cells at various stages of development, Liu et al.
298 observed a mixture of both the early mitotic-to-meiotic phenotype as well as a later phenotype
299 during late pachytene. Also, as Liu et al. administered tamoxifen in adult mice for five
300 consecutive days and analyzed the mice starting at two days post tamoxifen, the adult *Ythdc2*
301 cKO testes contained round and elongating spermatids in certain tubule stages likely from the
302 spermatogenic waves before tamoxifen introduction.

303 YTHDC2 contains several RNA-binding domains, including a R3H domain, RNA
304 helicase core module (DEXDc and HELICc motifs) and an OB fold. The RNA helicase domain
305 appears to be required for the function of YTHDC2 in late spermatogenesis, as a point mutation
306 in the YTHDC2 ATPase motif blocked meiotic prophase progress but not meiotic entry (Li et al.,

307 2022; Saito et al., 2022). YTHDC2 has been shown to have ATP-dependent, 3′ → 5′ RNA
308 unwinding activity (Jain et al., 2018; Wojtas et al., 2017). The YTHDC2 ATPase point mutant
309 phenotype appears similar to the later phenotype we and Liu et al. observed in *Ythdc2* cKO mice
310 rather than the earlier, mitosis-to-meiosis phenotype seen in *Ythdc2* null mutants, indicating that
311 YTHDC2's helicase activity is required for is function in late pachytene spermatocytes but not in
312 early spermatocytes. YTHDC2 also contains an YT521-B homology (YTH) domain that is not
313 present in *Drosophila Bgcn*. The YTH domain of all five YTH family members can specifically
314 recognize the N^6-methyladenosine (m^6A) RNA modification (Xu et al., 2015). YTHDC2 has
315 been shown to preferentially bind m^6A modified RNAs (Hsu et al., 2017; Kretschmer et al.,
316 2018; Wojtas et al., 2017), although with much weaker affinity than other YTH domain proteins
317 (Xu et al., 2015). However, binding of the m^6A modification does not appear be critical for
318 YTHDC2 function in the testis, as disrupting the YTH domain did not lead to any defects in
319 spermatogenesis (Li et al., 2022; Saito et al., 2022).
320 Taken together, the data from our lab and others suggest that YTHDC2 may be playing
321 two different functional roles in early versus late meiotic prophase. We and others have shown
322 that a primary initial role of YTHDC2 in male germ cells entering meiotic prophase is to
323 destabilize mitotic transcripts, including *Cyclin A2* (Bailey et al., 2017; Hsu et al., 2017; Soh et
324 al., 2017; Wojtas et al., 2017). We now show here, using a conditional knockout strategy to
325 bypass the first functional requirement, that YTHDC2 plays a key second role in pachytene
326 spermatocytes.
327 Our RNA-seq data in P16 *Ythdc2* cKO testes identified the earliest transcript changes
328 upon *Ythdc2* knockout in spermatocytes. Interestingly, a large percentage (76%) of the top 25
329 most significant differentially expressed genes were direct targets of YTHDC2 based on analysis

330 by CLIP (Li et al., 2022; Saito et al., 2022). Of the 19 YTHDC2 target mRNAs in this group,
331 five were detected at higher levels in P16 *Ythdc2* cKO testes compared to controls (*Sphkap*,
332 *Meioc*, *Zpbp, C1galt1* and *Slc16a7*). The remaining 14 target mRNAs were detected at lower
333 levels in P16 *Ythdc2* cKO testes compared to controls, suggesting that these key dysregulated
334 transcripts may be stabilized directly by YTHDC2 during meiotic prophase.

335 While post-transcriptional regulation through action of YTHDC2 may alter RNA
336 abundance for some YTHDC2 targets, we found that the changes in transcript levels by RNA-
337 sequencing in both the *Ythdc2* null mutant (Bailey et al., 2017) and the *Ythdc2* cKO were often
338 quantitatively small, and many direct YTHDC2 RNA targets identified by CLIP in both early
339 (Saito et al., 2022) and late (Li et al., 2022; Saito et al., 2022) spermatocytes showed no changes
340 in RNA expression levels at the time points we assessed, suggesting that binding of YTHDC2
341 could affect other processes, such as promoting or repressing translation or regulating
342 localization or storage of the target RNAs. Previous studies have suggested that YTHDC2 could
343 promote translation of certain RNA targets, as YTHDC2 interacts with the small ribosomal
344 subunit (Kretschmer et al., 2018) and binding of YTHDC2 to transcript coding sequences (CDS)
345 may help resolve mRNA secondary structures and promote translation *in vitro* (Mao et al.,
346 2019). While a recent study performed ribosome profiling on P8 and P10 testes and found that
347 loss of *Ythdc2* did not substantially alter the translation of YTHDC2 targets (Saito et al., 2022),
348 indicating that YTHDC2 likely does not regulate translation of its targets at the mitotic to
349 meiotic switch, it remains to be determined whether YTHDC2 may act through translational
350 regulation in late spermatocytes. YTHDC2 CLIP experiments from P8, P10 and adult testes
351 suggest that the RNA targets may vary across germ cell stages (Saito et al., 2022). Therefore,
352 YTHDC2 action on target RNAs could be different depending on factors such as where on the

353 transcript YTHDC2 binds (CDS versus 3′UTR) (Li et al., 2022; Mao et al., 2019; Saito et al.,
354 2022) or what other YTHDC2-binding partners are present when the target RNA is bound.
355 Several studies have previously determined that YTHDC2 is part of a protein complex
356 containing MEIOC (Abby et al., 2016; Bailey et al., 2017; Soh et al., 2017), the RNA-binding
357 protein RMB46 (Li et al., 2022; Qian et al., 2022) as well as the exoribonuclease XRN1
358 (Kretschmer et al., 2018; Li et al., 2022; Wojtas et al., 2017). To elucidate the mechanism(s) of
359 action of YTHDC2 during early and late meiotic prophase, we performed YTHDC2
360 immunoprecipitation experiments in P12 and P18 testis extracts, which revealed both RNA-
361 independent and RNA-dependent YTHDC2 interacting partners in early and late spermatocytes.
362 All the YTHDC2-bound interacting proteins we detected have known roles in regulating RNA
363 biology, consistent with the proposed functional role of YTHDC2 in regulating gene expression
364 through regulation of target RNAs. YTHDC2 may associate with specific protein complexes at
365 different cell stages, leading to diverse, stage-specific molecular outcomes on RNA targets.
366 Similar RBM46 IP Mass-spec experiments performed in P12 and P21 mouse testes revealed a
367 number of RBM46-associated proteins, several of which were also present in the YTHDC2
368 protein complexes we identified, including MEIOC, PABPC1, MOV10 and UPF1 (Qian et al.,
369 2022).
370 In our previous study examining the subcellular localization of YTHDC2, we showed
371 that while YTHDC2 is distributed throughout the cytoplasm, it also concentrated in perinuclear
372 puncta that co-expressed the P-body marker DCP1A (Bailey et al., 2017). Here we show that
373 MEIOC protein strongly accumulated in cytoplasmic puncta that co-expressed the granule
374 markers DCP1A and MIWI in *Ythdc2* cKO testis tubules. Interestingly, MEIOC protein did not
375 appear as enriched in cytoplasmic puncta in control spermatocytes. One explanation for why

376 knockout of *Ythdc2* in spermatocytes leads to increased MEIOC in puncta could be that
377 YTHDC2 is directly acting to move MEIOC out of the granules in pachytene spermatocytes.
378 Alternatively, MEIOC accumulation in granules could be an indirect effect of YTHDC2
379 deficiency. For example, other MEIOC binding partners could facilitate increased puncta
380 localization in the absence of YTHDC2. In addition to YTHDC2 and MEIOC, all of the
381 additional protein interacting partners identified in this study have also been shown to be
382 components of P-bodies or other types of RNP granules. Taken together, these data suggest that
383 the YTHDC2 complex may recruit target RNAs into granules where they are degraded,
384 translationally silenced or stored depending on the components of the granule, and/or return
385 target RNAs from granules to the cytoplasm where they can be translated.
386 The conserved mouse proteins YTHDC2, MEIOC and RBM46 function together to
387 regulate proper entry and execution of the mitosis-to-meiosis transition. All three proteins play a
388 critical role at the switch, as germ cells null mutant for any of the three proteins attempt to enter
389 the meiotic program but fail to shut off the mitotic program. As our current data reveal that
390 YTHDC2 has an additional role in late spermatocytes, it would be interesting to examine
391 whether MEIOC and RBM46 also function during late meiotic prophase, or if YTHDC2 may
392 instead work with other proteins to facilitate the transition from late pachytene to diplotene
393 spermatocytes.

394 **MATERIALS AND METHODS**

395 **Mice**

396 *Ythdc2* conditional knockout mice were generated according to the scheme depicted in Figure 1-
397 figure supplement 1. *Ythdc2*$^{tp/tp}$ mice (Bailey et al., 2017) were crossed to C57BL/6N-Tg(CAG-
398 Flpo)1Afst/Mmucd (RRID:MMRRC_036512-UCD) mice which removed the gene-trap cassette
399 by Flp recombinase and reverted the mutation to wild type, with LoxP sites flanking exons 6 and
400 7 (*Ythdc2*^{flox}). Removal of the gene-trap cassette was confirmed by PCR using the following
401 primers: *Ythdc2* forward 5′arm: 5′-CTGAACATGTCTTATCCACAGTGC-3′, *Ythdc2* reverse
402 3′arm: 5′- CATCATCAAGAAGGTTACAACAGGC-3′, Neo forward: 5′-
403 CAGCGCATCGCCTTCTATCGCC-3′. The *Ythdc2*^{flox} mice were then crossed to mice carrying
404 the *Ythdc2* null allele (*Ythdc2*$^{+/\Delta}$) (Bailey et al., 2017) to generate *Ythdc2*$^{flox/\Delta}$ mice. *Ythdc2*$^{flox/\Delta}$
405 mice were crossed to either the inducible Cre strain *B6.Cg-Ndor1*$^{Tg(UBC\text{-}cre/ERT2)1Ejb}$*/1J*
406 (RRID:IMSR_JAX:007001) (Ruzankina et al., 2007) or to *Tg(Spo11-cre)1Rsw/PecoJ*
407 (RRID:IMSR_JAX:032646) (Lyndaker et al., 2013). Mice were genotyped by PCR using the
408 following primers: *Cre* forward: 5′- TGGGCGGCATGGTGCAAGTT -3′, *Cre* reverse: 5′-
409 CGGTGCTAACCAGCGTTTTC -3′, *Ythdc2* forward: 5′-
410 CGAGTGCTGCCTTGGATGTGAACC -3′, *Ythdc2* reverse: 5′-
411 GGATTTTGACAGCCTTGAGCCTGGG -3′, targeting cassette (*LacZ*) forward: 5′-
412 GAATTATGGCCCACACCAGTGGCG -3′. All experiments were approved by the Stanford
413 University Animal Care and Use Committee and performed according to NIH guidelines.

414 ***Ythdc2* knockout with Tamoxifen**

415 Tamoxifen (10 mg/ml, Cayman Chemical) was dissolved in corn oil by incubating at 55°C for 40
416 min with constant rotation and then 0.1 mg/g body weight was injected intraperitoneally using a

417 27G needle into *UBC-Cre*^{ERT2}*;Ythdc2*$^{flox/\Delta}$ mice at P12 and P13 at the same time each day.

418 *Ythdc2*$^{flox/\Delta}$ male mice lacking *UBC-Cre*^{ERT2} were injected with tamoxifen and used as controls.

419 **Histology**

420 Mouse testes were fixed overnight at room temperature (RT) in bouins fixative and embedded in

421 paraffin. Paraffin-embedded samples were cut to 5-6 μm sections and stained with periodic acid-

422 Schiff (PAS).

423 **Immunofluorescence**

424 For immunofluorescence staining, tissues were fixed with 4% paraformaldehyde overnight at

425 4°C, embedded in paraffin and cut to 5-6 μm thickness. After rehydrating in an ethanol gradient,

426 heat-mediated antigen retrieval was performed on the sections using sodium citrate buffer (10

427 mM sodium citrate, 0.05% Tween-20, pH 6.0). Sections were then permeabilized with

428 phosphate-buffered saline + 0.1% TritonX-100 (PBST) for 45 min at RT, followed by 1 hr

429 incubation with blocking buffer (10% BSA in PBST) at RT. Sections were incubated with

430 primary antibody overnight at 4°C and then incubated with Alexa Fluor-conjugated donkey

431 secondary antibodies (1:400, Molecular Probes) at RT for 2 hrs and then mounted in

432 VECTASHIELD medium with 4′-6-Diamidino-2-phenylindole (DAPI) (Vector Lab Inc.).

433 When immunolabeling with antibodies from the same host species, following incubation with

434 primary antibody overnight at 4°C, slides were washed 3 times in PBS, and then incubated with

435 HRP anti-rabbit IgG (1:500 in 10% BSA in PBST) for 1 hr at RT. Following incubation, TSA

436 plus cyanine 3 solution (dilute TSA-Cy3 1:250 in 100mM Boric Acid, pH8.5 containing 0.003%

437 H_2O_2) (Akoya Biosciences) was added to the tissue sections and incubated for 10 min at RT.

438 Slides were then washed twice in PBS and antigen retrieval using sodium citrate buffer was

439 performed a second time. Sections were blocked and then incubated with primary and secondary
440 antibodies as described above.

441 **Antibodies**

442 Rabbit anti-YTHDC2 (1:500 or 1:2,000 when TSA used, A303-026A, (RRID:AB_10754785),
443 Bethyl laboratories), mouse anti-SYCP3 (1:200, clone [Cor 10G11/7], (RRID:AB_10678841),
444 Abcam), rabbit anti-SYCP3 (1:500, NB300-232, (RRID:AB_2087193), Novus Biologicals),
445 rabbit anti-RAD51 (1:200 [N1C2], (RRID:AB_1951602) , GeneTex), goat anti-VASA (1:200,
446 AF2030, (RRID:AB_2277369), R&D Systems), mouse anti-phospho-Histone H2A.X (Ser139)
447 (1:500 clone [JBW301], (RRID:AB_309864), Millipore), rabbit anti-CYCLIN A2 (1:250 clone
448 [EPR17351], (RRID:AB_2890136), Abcam), rabbit anti-MEIOC (1:1,000 IF David Page Lab),
449 mouse anti-DCP1A (1:250 clone [3G4], (RRID:AB_1843673), Sigma), goat anti-PIWIL1
450 (1:200, AF6548, (RRID:AB_10971944), Novus Biologicals). Terminal deoxynucleotidyl
451 transferase dUTP nick end labeling (TUNEL) staining was done following manufacturer's
452 instruction (In Situ cell Death Detection Kit TMR red, Roche).

453 The following antibodies were used for immunoblot: rabbit anti-YTHDC2 (1:1,000, A303-026A,
454 (RRID:AB_10754785), Bethyl laboratories), rabbit anti-MEIOC (1:2000 immunoblot, David
455 Page Lab), goat anti-RENT1/UPF1 (1:2,000, A300-038A, (RRID:AB_2288326), Bethyl
456 laboratories), rabbit anti-EWS (1:2,000, A300-417A, (RRID:AB_420957), Bethyl laboratories),
457 rabbit anti-MOV10 (1:2,000, A301-571A, (RRID:AB_1040002), Bethyl laboratories), rabbit
458 anti-G3BP2 (1:2,000, A302-040A, (RRID:AB_1576545), Bethyl laboratories), rabbit anti-YBX1
459 (1:2,000, A303-231A, (RRID:AB_10951283), Bethyl laboratories), mouse anti-PTBP1 (1:2,000,
460 Thermo), rabbit anti-PABPC1 (1:1,000, ab21060, (RRID:AB_777008, Abcam), rabbit anti-

461 FMR1 (1:2,000, A305-200A, (RRID:AB_2631593), Bethyl laboratories), rabbit anti-CAPRIN1
462 (1:2,000, HPA018126, (RRID:AB_1849929), Sigma).

463 **Germ-cell spreads**

464 Chromosome spreads from P16 and P18 testes were performed based on a previously published
465 protocol (Peters et al., 1997). Briefly, testis tubules were incubated in a hypotonic extraction
466 buffer pH 8.2 (30 mM Tris-HCL pH 8.0, 50 mM sucrose, 17 mM trisodium citrate dehydrate, 5
467 mM EDTA, 0.5 mM DTT, 0.5 mM PMSF) for 30 min. Testis tubules were then broken apart in
468 100 mM sucrose pH 8.2 and then spread on a slide dipped in fixation buffer pH 9.2 (1% PFA and
469 0.15% Triton X-100). Slides were incubated overnight in a humidified chamber at RT and air-
470 dried. Slides were washed twice in 0.4% Photoflo (Kodak) and air-dried.

471 **Co-immunoprecipitation from testes**

472 Anti-YTHDC2 (A303-025A, Bethyl laboratories) was conjugated to Protein A Dynabeads
473 (Invitrogen). Dynabeads (50 μL/IP) were blocked briefly in 3% BSA in PBS + 0.1% tween 20
474 (PBST) and then incubated at 4°C overnight in lysis buffer (20 mM Tris-HCL, 135 mM NaCl,
475 10% glycerol, 1% Nonidet P-40, 5 mM EDTA) plus 2 μg YTHDC2 antibody. Beads were
476 washed three times with 0.2 M triethanolamine, pH 8.2 for 5 min at RT, then incubated with
477 dimethylprimelimidate (DMP, 5.4 mg DMP per mL 0.2 M triethanolamine, Sigma) for 30 min at
478 RT. Beads were washed once with 50 mM Tris for 15 min, followed by three 5-min washes with
479 PBST. Crosslinked beads can be stored overnight at 4°C or used immediately in the next step. To
480 remove un-crosslinked antibody, beads were quickly washed twice with 100mM glycine, pH2.5,
481 then blocked in 3% BSA PBST for 30 min followed by three quick PBST washes.
482 For immunoprecipitations from testis extracts, testes were dissected from P12 and P18 wild-type
483 mice. Testis extracts were prepared by mechanically disrupting testes in lysis buffer (20 mM

484 Tris-HCL, 135 mM NaCl, 10% glycerol, 1% Nonidet P-40, 5 mM EDTA, 1 mM PMSF, 1x
485 Complete protease inhibitor, and either (A) 100 U/mL RNAse-OUT or (B) 50 µg/mL RNAse A).
486 Extracts were incubated in lysis buffer for 20 min at 4°C, spun for 20 min, and then precleared
487 with uncoupled, 3% BSA-blocked Protein A Dynabeads for 1 hr at 4°C. Testis extracts were then
488 added to the crosslinked YTHDC2 antibody - Protein A Dynabeads and incubated for 3 hrs at
489 4°C while rotating. Beads were washed three times in lysis buffer for 5 min each wash, and
490 incubated at 70°C for 30 min in elution buffer (1% SDS, 10 mM EDTA, 50 mM Tris pH 8.0, 1
491 mM PMSF, 1x Complete protease inhibitor) with frequent mixing. Samples were resolved on a
492 10% SDS-PAGE gel (Bio-Rad) and transferred onto polyvinylidene fluoride (PVDF)
493 membranes. Blots were then incubated in primary antibodies overnight at 4°C and then IgG HRP
494 secondary antibodies (1:10,000) for 2 hrs at RT and then developed using western lightning ECL
495 detection reagent.

496 **Mass-Spectometry**

497 Testes were dissected from P12 and P18 wild-type and *Ythdc2* mutant mice. YTHDC2
498 immunoprecipitations were performed as described above with slight modifications: the
499 uncoupled, preclear Protein A Dynabeads were washed with PBST to remove unbound BSA
500 prior to adding to the testis lysate, and the crosslinked YTHDC2 antibody - Protein A Dynabeads
501 were not blocked with 3% BSA following DMP crosslinking. Testis extracts were precleared
502 with uncoupled beads for 3 hrs at 4°C followed by incubation with the crosslinked YTHDC2
503 antibody - Protein A Dynabeads for 3 hrs at 4°C with continuous rotation. Beads were washed
504 three times in lysis buffer for 10 min each wash, and then incubated in elution buffer as
505 previously described above. Samples were resolved on a 10% SDS-PAGE gel (Bio-Rad). The
506 samples were allowed to run about 1 cm into the gel and the gel was then fixed for 1 hr in fixing

507 solution (45:45:10 / water:methanol:acetic acid) with gentle agitation. The samples were cut out
508 of the gel and stored at 4°C until being processed at the Stanford University Mass Spectrometry
509 Facility.

510 **RNA-seq from testes**

511 Testes were collected from P14 and P16 *UBC-Cre*^{ERT2}*;Ythdc2*$^{flox/\Delta}$ and *Ythdc2*$^{flox/\Delta}$ control mice
512 following tamoxifen injections at P12 and P13. One testis was snap frozen and the other was
513 fixed in 4% formaldehyde to confirm *Ythdc2* knockout. Total RNA was isolated from frozen
514 testes using the RNeasy Plus Mini Kit (Qiagen), according to manufacturer's instructions.
515 Ribosomal RNAs were depleted from 1 µg of total RNA using TruSeq Stranded Total RNA kit
516 Ribo-Zero components (Illumina) according to the manufacturer's protocol. Ribosomal-depleted
517 RNA was cleaned up using Agencourt RNAClean XP Beads (Beckman Coulter) and efficiency
518 of rRNA depletion was confirmed by bioanalyzer. Library preparation for high-throughput
519 sequencing was performed on 100 ng of rRNA depleted RNA using the NEBNext Ultra II
520 Directional RNA Library Prep Kit for Illumina (New England Biolabs). Sequencing was done
521 with a NextSeq 500/550 High Output Kit v2.5 (150 Cycles), with eight libraries pooled.
522 Approximately 55 million to 66 million reads were obtained per replicate and each condition had
523 two biological replicates.

524 **RNA expression analysis**

525 Libraries were separated by barcode and adapters and low-quality bases were trimmed using
526 trimGalore (Martin, 2011). Reads were mapped to the mouse genome (GRCm39/mm39) using
527 STAR (RRID:SCR_004463) (Dobin et al., 2013). Reads for each transcript were extracted using
528 HTSeq (RRID:SCR_005514) (Anders et al., 2015). Differential gene expression was calculated
529 using DESeq2 (RRID:SCR_015687) (Love et al., 2014).

530 **Statistical analysis**

531 Biological replicates were performed for RNA-Seq experiments and samples for each biological
532 replicate were collected from different animals. For phenotypic analysis, sample sizes (n) for
533 each experiment are given in the respective figure legends. Sample sizes used were similar to
534 what is generally utilized in the field. Each animal was considered a biological replicate. No
535 samples were excluded from analysis. All bar graphs are presented as means ± SEM. Statistical
536 differences between two groups were analyzed using unpaired two-tailed t tests; $p<0.05$ was
537 considered statistically significant.

538 **Data availability**

539 RNA-seq data have been deposited in the Gene Expression Omnibus (GEO) under accession
540 number GSE222283.

541 **ACKNOWLEDGEMENTS**

542 We thank members of the Fuller laboratory for many helpful discussions and feedback
543 throughout the project, David Page for providing the MEIOC antibody and Georgi Marinov for
544 running the high-throughput sequencing. We also thank the Stanford Comparative Medicine
545 Animal Histology Services for preparing histological sections, the Stanford Protein and Nucleic
546 Acid Facility for RNA quality control analysis, and the Vincent Coates Foundation Mass
547 Spectrometry Laboratory, Stanford University Mass Spectrometry core. This work was
548 supported by the National Institutes of Health (NIH T32 AR007422) to A.S.B., the National
549 Institutes of Health (R01 GM122951 and R35 GM136433), the Katharine Dexter McCormick
550 and Stanley McCormick Memorial Professorship and the Reed-Hodgson Professorship in Human
551 Biology to M.T.F., and the National Institutes of Health (NIH P30 CA124435) utilizing
552 the Stanford Cancer Institute Proteomics/Mass Spectrometry Shared Resource.

COMPETING INTERESTS

The authors have no competing interests.

555 **REFERENCES**

556 Abby, E., Tourpin, S., Ribeiro, J., Daniel, K., Messiaen, S., Moison, D., Guerquin, J., Gaillard,
557 J.C., Armengaud, J., Langa, F., Toth, A., Martini, E., and Livera, G. (2016). Implementation of
558 meiosis prophase I programme requires a conserved retinoid-independent stabilizer of meiotic
559 transcripts. Nature communications *7*, 10324. 10.1038/ncomms10324.

560 Anders, S., Pyl, P.T., and Huber, W. (2015). HTSeq--a Python framework to work with high-
561 throughput sequencing data. Bioinformatics *31*, 166-169. 10.1093/bioinformatics/btu638.

562 Bailey, A.S., Batista, P.J., Gold, R.S., Chen, Y.G., de Rooij, D.G., Chang, H.Y., and Fuller, M.T.
563 (2017). The conserved RNA helicase YTHDC2 regulates the transition from proliferation to
564 differentiation in the germline. eLife *6*. 10.7554/eLife.26116.

565 Chen, D., Wu, C., Zhao, S., Geng, Q., Gao, Y., Li, X., Zhang, Y., and Wang, Z. (2014). Three
566 RNA binding proteins form a complex to promote differentiation of germline stem cell lineage in
567 Drosophila. PLoS genetics *10*, e1004797. 10.1371/journal.pgen.1004797.

568 Dobin, A., Davis, C.A., Schlesinger, F., Drenkow, J., Zaleski, C., Jha, S., Batut, P., Chaisson,
569 M., and Gingeras, T.R. (2013). STAR: ultrafast universal RNA-seq aligner. Bioinformatics *29*,
570 15-21. 10.1093/bioinformatics/bts635.

571 Hsu, P.J., Zhu, Y., Ma, H., Guo, Y., Shi, X., Liu, Y., Qi, M., Lu, Z., Shi, H., Wang, J., Cheng,
572 Y., Luo, G., Dai, Q., Liu, M., Guo, X., Sha, J., Shen, B., and He, C. (2017). Ythdc2 is an N(6)-
573 methyladenosine binding protein that regulates mammalian spermatogenesis. Cell Res *27*, 1115-
574 1127. 10.1038/cr.2017.99.

575 Insco, M.L., Bailey, A.S., Kim, J., Olivares, G.H., Wapinski, O.L., Tam, C.H., and Fuller, M.T.
576 (2012). A self-limiting switch based on translational control regulates the transition from
577 proliferation to differentiation in an adult stem cell lineage. Cell Stem Cell *11*, 689-700.
578 10.1016/j.stem.2012.08.012.

579 Jain, D., Puno, M.R., Meydan, C., Lailler, N., Mason, C.E., Lima, C.D., Anderson, K.V., and
580 Keeney, S. (2018). ketu mutant mice uncover an essential meiotic function for the ancient RNA
581 helicase YTHDC2. eLife *7*. 10.7554/eLife.30919.

582 Kretschmer, J., Rao, H., Hackert, P., Sloan, K.E., Hobartner, C., and Bohnsack, M.T. (2018).
583 The m(6)A reader protein YTHDC2 interacts with the small ribosomal subunit and the 5'-3'
584 exoribonuclease XRN1. RNA *24*, 1339-1350. 10.1261/rna.064238.117.

585 Li, J., Mahajan, A., and Tsai, M.D. (2006). Ankyrin repeat: a unique motif mediating protein-
586 protein interactions. Biochemistry *45*, 15168-15178. 10.1021/bi062188q.

587 Li, L., Krasnykov, K., Homolka, D., Gos, P., Mendel, M., Fish, R.J., Pandey, R.R., and Pillai,
588 R.S. (2022). The XRN1-regulated RNA helicase activity of YTHDC2 ensures mouse fertility
589 independently of m(6)A recognition. Mol Cell *82*, 1678-1690 e1612.
590 10.1016/j.molcel.2022.02.034.

591 Liu, R., Kasowitz, S.D., Homolka, D., Leu, N.A., Shaked, J.T., Ruthel, G., Jain, D., Lin, H.,
592 Keeney, S., Luo, M., Pillai, R.S., and Wang, P.J. (2021). YTHDC2 is essential for pachytene
593 progression and prevents aberrant microtubule-driven telomere clustering in male meiosis. Cell
594 reports *37*, 110110. 10.1016/j.celrep.2021.110110.

595 Love, M.I., Huber, W., and Anders, S. (2014). Moderated estimation of fold change and
596 dispersion for RNA-seq data with DESeq2. Genome Biol *15*, 550. 10.1186/s13059-014-0550-8.

597 Lyndaker, A.M., Lim, P.X., Mleczko, J.M., Diggins, C.E., Holloway, J.K., Holmes, R.J., Kan,
598 R., Schlafer, D.H., Freire, R., Cohen, P.E., and Weiss, R.S. (2013). Conditional inactivation of
599 the DNA damage response gene Hus1 in mouse testis reveals separable roles for components of
600 the RAD9-RAD1-HUS1 complex in meiotic chromosome maintenance. PLoS genetics *9*,
601 e1003320. 10.1371/journal.pgen.1003320.

602 Mao, Y., Dong, L., Liu, X.M., Guo, J., Ma, H., Shen, B., and Qian, S.B. (2019). m(6)A in
603 mRNA coding regions promotes translation via the RNA helicase-containing YTHDC2. Nature
604 communications *10*, 5332. 10.1038/s41467-019-13317-9.

605 Martin, M. (2011). Cutadapt removes adapter sequences from high-throughput sequencing reads.
606 EMBnetjournal *17*, 10-12. 10.14806/ej.17.1.200.

607 Peart, N.J., Johnson, T.A., Lee, S., Sears, M.J., Yang, F., Quesnel-Vallieres, M., Feng, H.,
608 Recinos, Y., Barash, Y., Zhang, C., Hermann, B.P., Wang, P.J., Geyer, C.B., and Carstens, R.P.
609 (2022). The germ cell-specific RNA binding protein RBM46 is essential for spermatogonial
610 differentiation in mice. PLoS genetics *18*, e1010416. 10.1371/journal.pgen.1010416.

611 Peters, A.H., Plug, A.W., van Vugt, M.J., and de Boer, P. (1997). A drying-down technique for
612 the spreading of mammalian meiocytes from the male and female germline. Chromosome Res *5*,
613 66-68.

614 Qian, B., Li, Y., Yan, R., Han, S., Bu, Z., Gong, J., Zheng, B., Yuan, Z., Ren, S., He, Q., Zhang,
615 J., Xu, C., Wang, R., Sun, Z., Lin, M., Zhou, J., and Ye, L. (2022). RNA binding protein RBM46

616 regulates mitotic-to-meiotic transition in spermatogenesis. Sci Adv *8*, eabq2945.
617 10.1126/sciadv.abq2945.

618 Ruzankina, Y., Pinzon-Guzman, C., Asare, A., Ong, T., Pontano, L., Cotsarelis, G., Zediak, V.P.,
619 Velez, M., Bhandoola, A., and Brown, E.J. (2007). Deletion of the developmentally essential
620 gene ATR in adult mice leads to age-related phenotypes and stem cell loss. Cell Stem Cell *1*,
621 113-126. 10.1016/j.stem.2007.03.002.

622 Saito, Y., Hawley, B.R., Puno, M.R., Sarathy, S.N., Lima, C.D., Jaffrey, S.R., Darnell, R.B.,
623 Keeney, S., and Jain, D. (2022). YTHDC2 control of gametogenesis requires helicase activity
624 but not m(6)A binding. Genes & development *36*, 180-194. 10.1101/gad.349190.121.

625 Soh, Y.Q.S., Mikedis, M.M., Kojima, M., Godfrey, A.K., de Rooij, D.G., and Page, D.C. (2017).
626 Meioc maintains an extended meiotic prophase I in mice. PLoS genetics *13*, e1006704.
627 10.1371/journal.pgen.1006704.

628 Wojtas, M.N., Pandey, R.R., Mendel, M., Homolka, D., Sachidanandam, R., and Pillai, R.S.
629 (2017). Regulation of m(6)A Transcripts by the 3'-->5' RNA Helicase YTHDC2 Is Essential for
630 a Successful Meiotic Program in the Mammalian Germline. Mol Cell *68*, 374-387 e312.
631 10.1016/j.molcel.2017.09.021.

632 Xu, C., Liu, K., Ahmed, H., Loppnau, P., Schapira, M., and Min, J. (2015). Structural Basis for
633 the Discriminative Recognition of N6-Methyladenosine RNA by the Human YT521-B
634 Homology Domain Family of Proteins. The Journal of biological chemistry *290*, 24902-24913.
635 10.1074/jbc.M115.680389.
636

Figure 1.

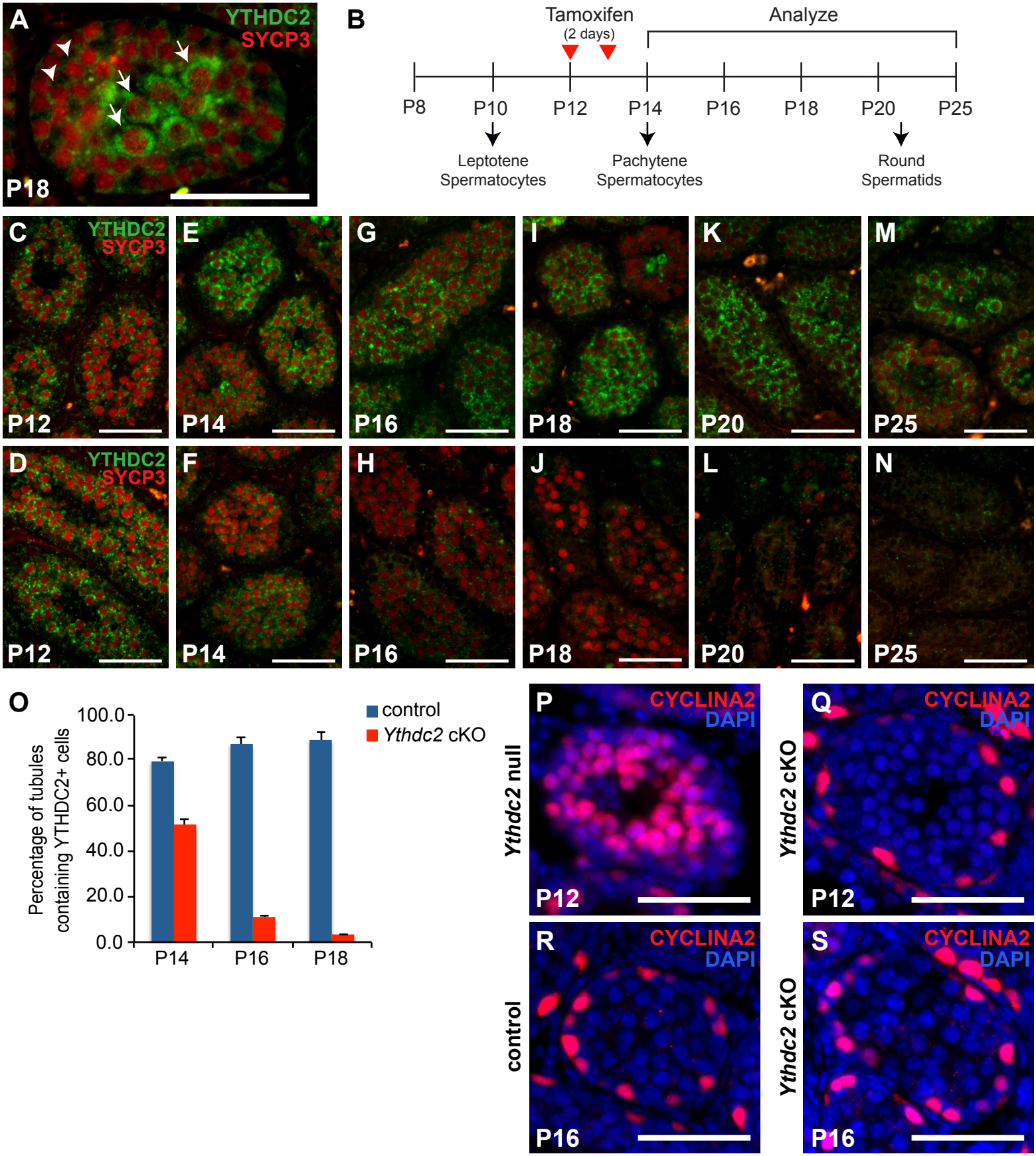
A
YTHDC2
SYCP3
P18
B
Tamoxifen
(2 days)
Analyze
P8
P10
P12
P14
P16
P18
P20
P25
Leptotene
Spermatocytes
Pachytene
Spermatocytes
Round
Spermatids
control
Ythdc2 cKO
C
E
G
I
K
M
D
F
H
J
L
N
O
Percentage of tubules containing YTHDC2+ cells
100.0
80.0
60.0
40.0
20.0
0.0
control
Ythdc2 cKO
Ythdc2 null
P
Q
R
S
CYCLINA2
DAPI

637 **Figure 1. Knockout of *Ythdc2* in late spermatocytes during the first wave of**
638 **spermatogenesis.** (A) Immunofluorescence image of a P18 wild-type mouse testis tubule cross-
639 section stained for YTHDC2 (green) and SYCP3 (red). Arrowheads: leptotene spermatocytes
640 from the second wave of spermatogenesis. Arrows: pachytene spermatocytes from the first wave
641 of spermatogenesis within the lumen of the testis tubule. (B) Diagram of the appearance of germ
642 cell stages during the first wave of spermatogenesis and the timing of tamoxifen injections and
643 analysis of control and *Ythdc2* cKO mice. (C-N) Immunofluorescence images of control (+/+;
644 *Ythdc2*$^{flox/\Delta}$, top) and *Ythdc2* cKO (*UBC-CreERT2; Ythdc2*$^{flox/\Delta}$, bottom) seminiferous tubule
645 cross-sections from (C, D) P12, (E, F) P14, (G, H) P16, (I, J) P18, (K, L) P20 and (M, N) P25
646 testes stained for YTHDC2 (green) and SYCP3 (red). (O) Percentage of tubules containing
647 YTHDC2-positive cells in P14, P16 and P18 control (blue) and *Ythdc2* cKO (red) testes (n = 2-4
648 mice per group; t test, P14: p-value = 0.0003, P16: p-value < 0.0001, P18: p-value = 0.0019).
649 Error bars: SEM. (P-S) Immunofluorescence images of testis tubules from (P) P12 *Ythdc2* null
650 (Q) P12 *Ythdc2* cKO (R) P16 control and (S) P16 *Ythdc2* cKO mice stained for CYCLINA2
651 (red) and DAPI (blue). Scale bars: 50 µm. See also Figure 1-figure supplement 1.

Figure 2.

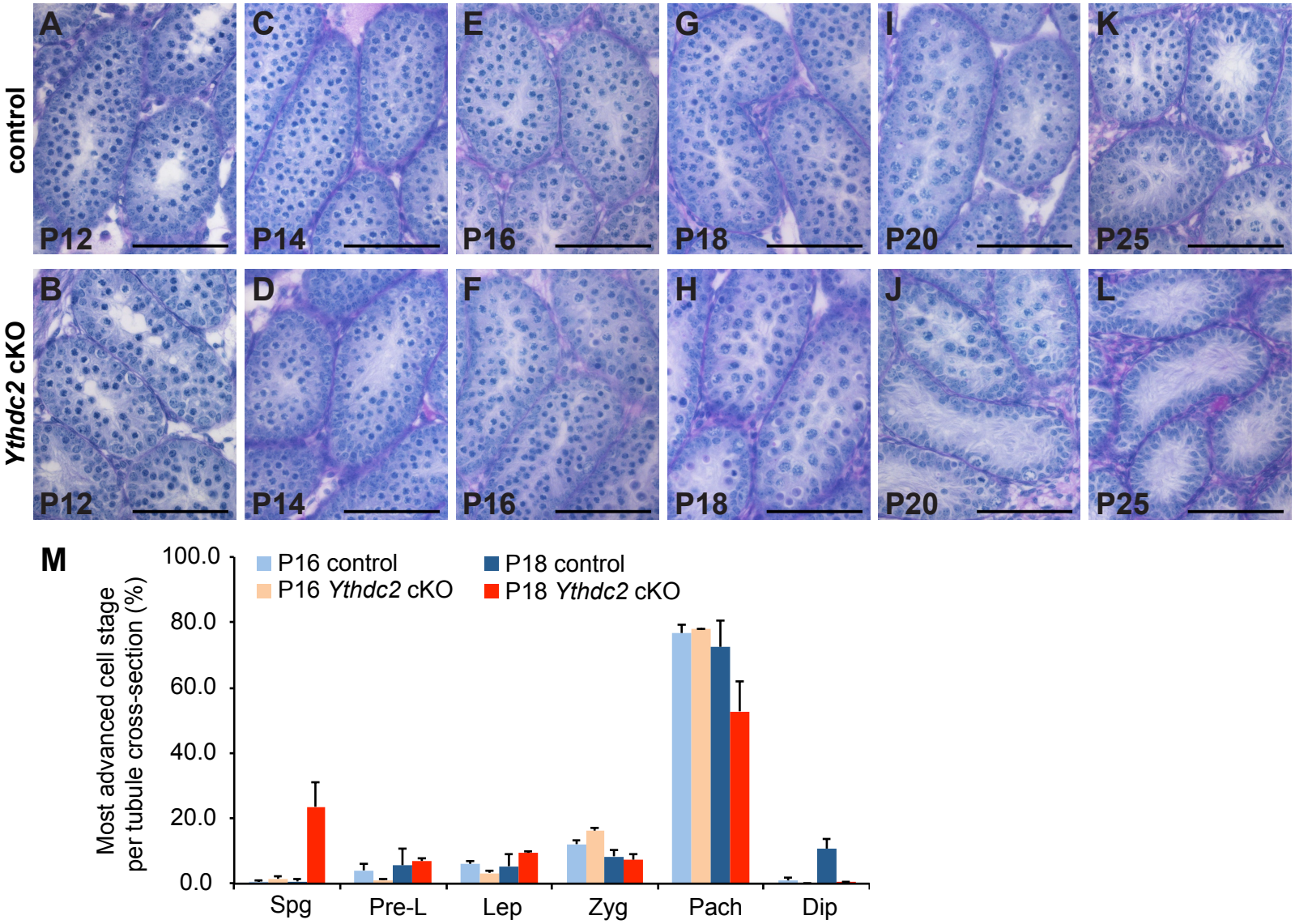
control
Ythdc2 cKO
A
B
C
D
E
F
G
H
I
J
K
L
P12
P14
P16
P18
P20
P25
M
P16 control
P16 Ythdc2 cKO
P18 control
P18 Ythdc2 cKO
Most advanced cell stage per tubule cross-section (%)
100.0
80.0
60.0
40.0
20.0
0.0
Spg
Pre-L
Lep
Zyg
Pach
Dip

652 **Figure 2. YTHDC2 is required for late spermatocytes to progress through meiotic**
653 **prophase.** (A-L) Sections of mouse seminiferous tubules stained with periodic acid-Schiff (PAS)
654 from (A, B) P12, (C, D) P14, (E, F) P16, (G, H) P18, (I, J) P20 and (K, L) P25 control (+/+*;*
655 *Ythdc2*$^{flox/\Delta}$, top) and *Ythdc2* cKO (*UBC-CreERT2; Ythdc2*$^{flox/\Delta}$, bottom) testis. Scale bars: 50 µm.
656 (M) Percentage of tubule cross-sections containing spermatogonia (Spg), preleptotene (Pre-L),
657 leptotene (Lep), zygotene (Zyg), pachytene (Pach) or diplotene (Dip) as the most advanced cell
658 stage in P16 control (light blue), P16 *Ythdc2* cKO (light orange), P18 control (blue) and P18
659 *Ythdc2* cKO (red) testes (n = 2 mice per group; > 115 tubules counted per cross-section). Error
660 bars: SEM.

Figure 3.

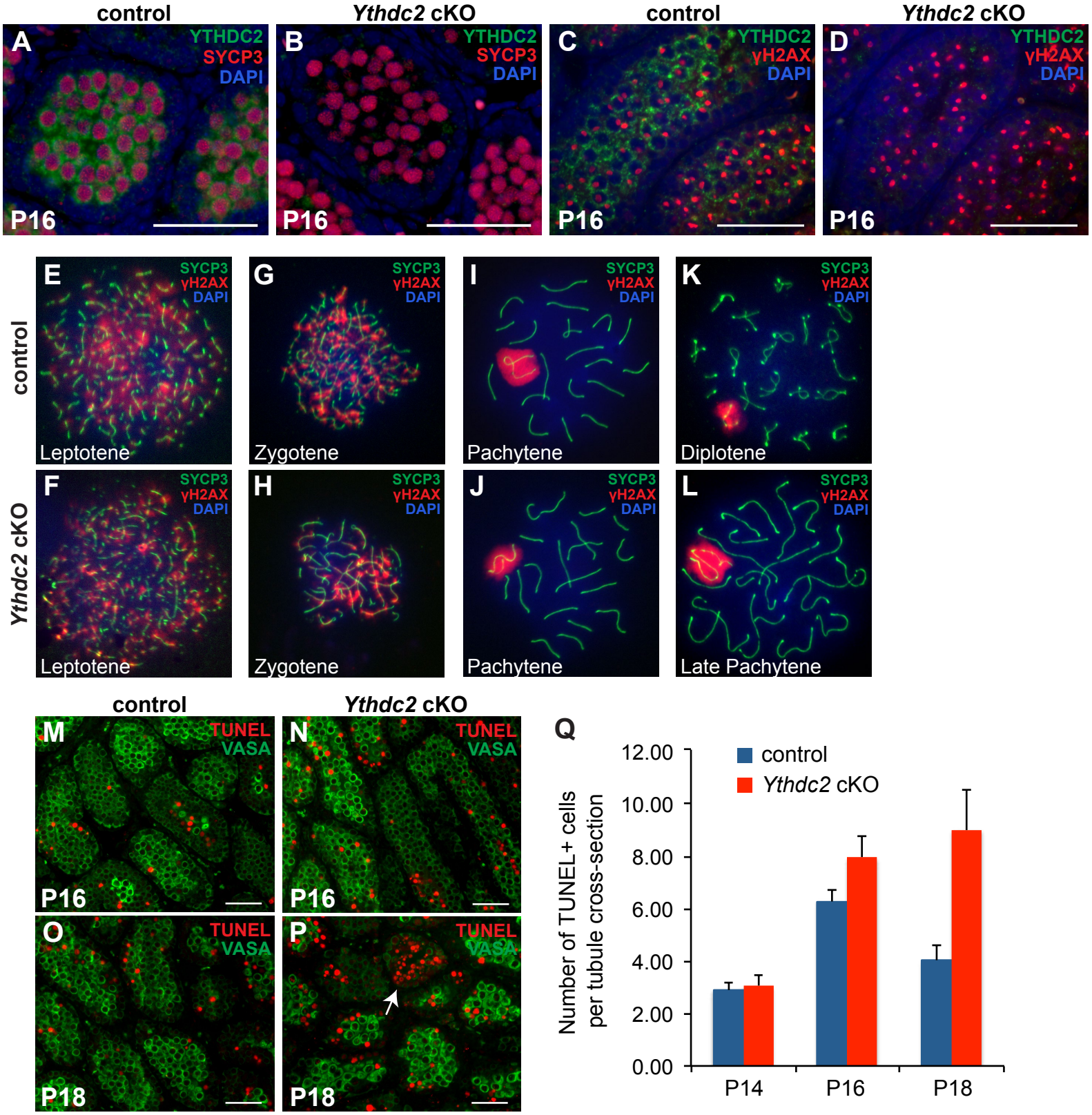
control
Ythdc2 cKO
control
Ythdc2 cKO
A
YTHDC2
SYCP3
DAPI
P16
B
YTHDC2
SYCP3
DAPI
P16
C
YTHDC2
γH2AX
DAPI
P16
D
YTHDC2
γH2AX
DAPI
P16
control
Ythdc2 cKO
E
SYCP3
γH2AX
DAPI
Leptotene
G
SYCP3
γH2AX
DAPI
Zygotene
I
SYCP3
γH2AX
DAPI
Pachytene
K
SYCP3
γH2AX
DAPI
Diplotene
F
SYCP3
γH2AX
DAPI
Leptotene
H
SYCP3
γH2AX
DAPI
Zygotene
J
SYCP3
γH2AX
DAPI
Pachytene
L
SYCP3
γH2AX
DAPI
Late Pachytene
control
Ythdc2 cKO
M
TUNEL
VASA
P16
N
TUNEL
VASA
P16
O
TUNEL
VASA
P18
P
TUNEL
VASA
P18
Q
control
Ythdc2 cKO
Number of TUNEL+ cells per tubule cross-section
12.00
10.00
8.00
6.00
4.00
2.00
0.00
P14
P16
P18

661 **Figure 3. Spermatocytes lacking YTHDC2 reach the pachytene stage but then quickly die.**

662 (A, B) Testis from P16 (A) control (+/+; *Ythdc2*$^{flox/\Delta}$) and (B) *Ythdc2* cKO (*UBC-CreERT2;*

663 *Ythdc2*$^{flox/\Delta}$) mice stained for YTHDC2 (green), SYCP3 (red) and DAPI (blue). (C, D) Testis

664 from P16 (C) control and (D) *Ythdc2* cKO mice stained for YTHDC2 (green), γH2AX (red) and

665 DAPI (blue). (E-L) Immunofluorescence images of germ cell spreads from P18 control (top) and

666 *Ythdc2* cKO (bottom) mice stained for SYCP3 (green), γH2AX (red) and DAPI (blue). (M-P)

667 Testis tubule cross-sections from (M, N) P16 and (O, P) P18 control and *Ythdc2* cKO mice

668 labeled with TUNEL (red) and VASA (green). Arrow: Tubule filled with TUNEL-positive cells.

669 Scale bars: 50 µm. (Q) Number of TUNEL-positive cells per tubule cross-section in P14, P16

670 and P18 control (blue) and *Ythdc2* cKO (red) testes (n = 2-3 mice per group). Error bars: SEM.

671 See also Figure 3-figure supplement 1 and Figure 3-figure supplement 2.

Figure 4.

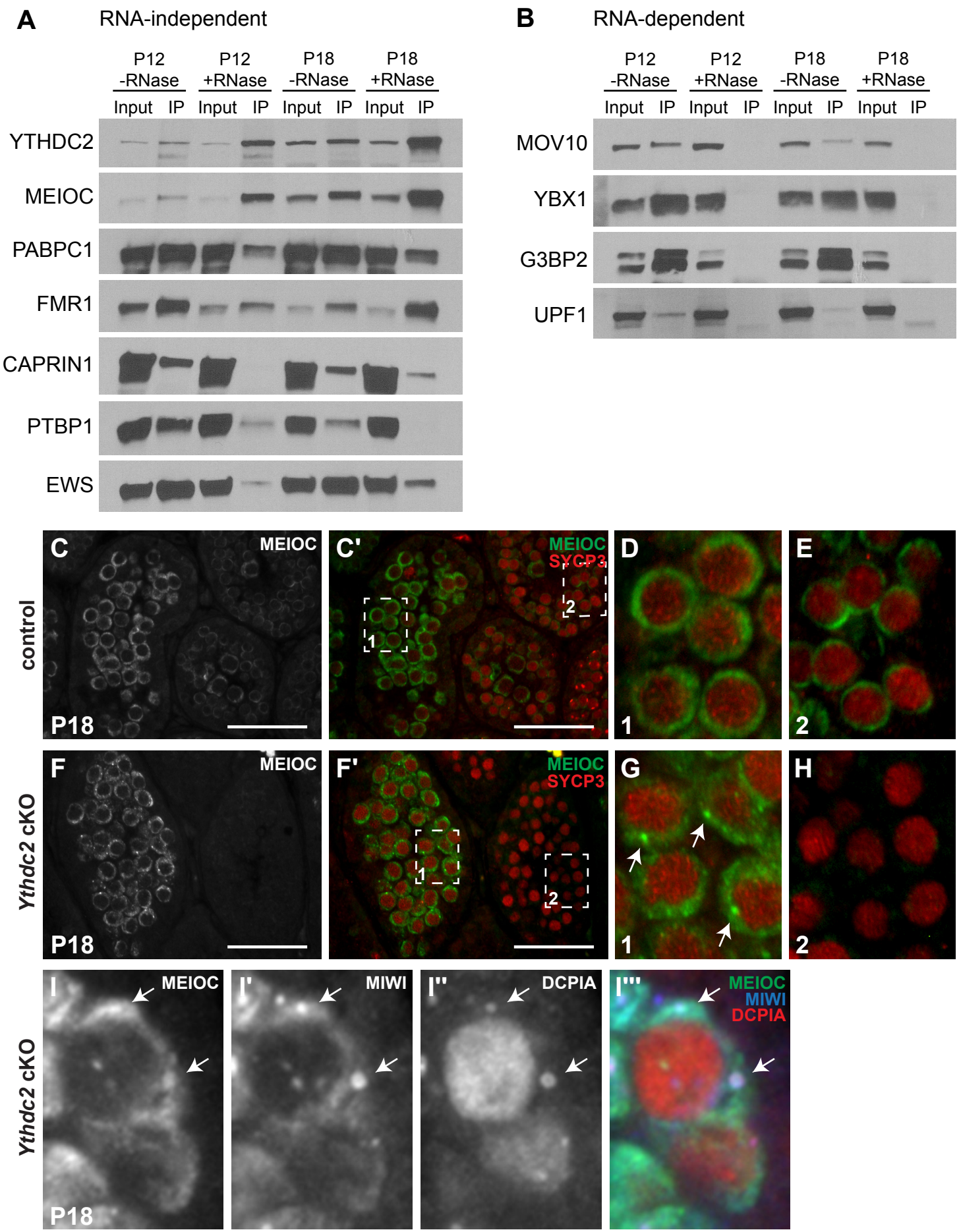
A
RNA-independent
P12 -RNase
P12 +RNase
P18 -RNase
P18 +RNase
Input IP Input IP Input IP Input IP
YTHDC2
MEIOC
PABPC1
FMR1
CAPRIN1
PTBP1
EWS
B
RNA-dependent
P12 -RNase
P12 +RNase
P18 -RNase
P18 +RNase
Input IP Input IP Input IP Input IP
MOV10
YBX1
G3BP2
UPF1
control
C
MEIOC
P18
C'
MEIOC
SYCP3
1
2
D
1
E
2
Ythdc2 cKO
F
MEIOC
P18
F'
MEIOC
SYCP3
1
2
G
1
H
2
Ythdc2 cKO
I
MEIOC
P18
I'
MIWI
I''
DCPIA
I'''
MEIOC
MIWI
DCPIA

672 **Figure 4. YTHDC2 interacts with several other proteins involved in RNA regulation.**
673 (A, B) Immunoprecipitation with α-YTHDC2 from P12 and P18 wild-type mouse testis extracts
674 containing either an RNase Inhibitor (-RNase) or RNase A (+RNase). Western blots probed with
675 α-YTHDC2, α-MEIOC, α-PABPC1, α-FMR1, α-CAPRIN1, α-PTBP1, α-EWS, α-MOV10, α-
676 YBX1, α-G3BP2 and α-UPF1. (C-H) Immunofluorescence images of testis cross-sections from
677 P18 (C-E) control (+/+; *Ythdc2*$^{flox/\Delta}$) and (F-H) *Ythdc2* cKO (*UBC-CreERT2; Ythdc2*$^{flox/\Delta}$) mice
678 stained for MEIOC (green) and SYCP3 (red). Scale bars: 50 µm. (D, E) High-magnification
679 images of (D) pachytene spermatocytes in boxed region 1 in panel C′ and (E) leptotene
680 spermatocytes in boxed region 2 in panel C′. (G, H) High-magnification image of (G) pachytene
681 spermatocytes in boxed region 1 in panel F′ and (H) leptotene spermatocytes in boxed region 2
682 in panel F′. Arrows: MEIOC protein in perinuclear puncta in pachytene spermatocytes. (I-I′′′)
683 High-magnification immunofluorescence images of spermatocytes from a P18 *Ythdc2* cKO
684 mouse testis cross-section stained for MEIOC (green), MIWI (blue) and DCP1A (red). Arrows:
685 puncta in the cytoplasm of pachytene spermatocytes. See also Figure 4 – source data 1 and
686 Figure 4 – source data 2.

Figure 5.

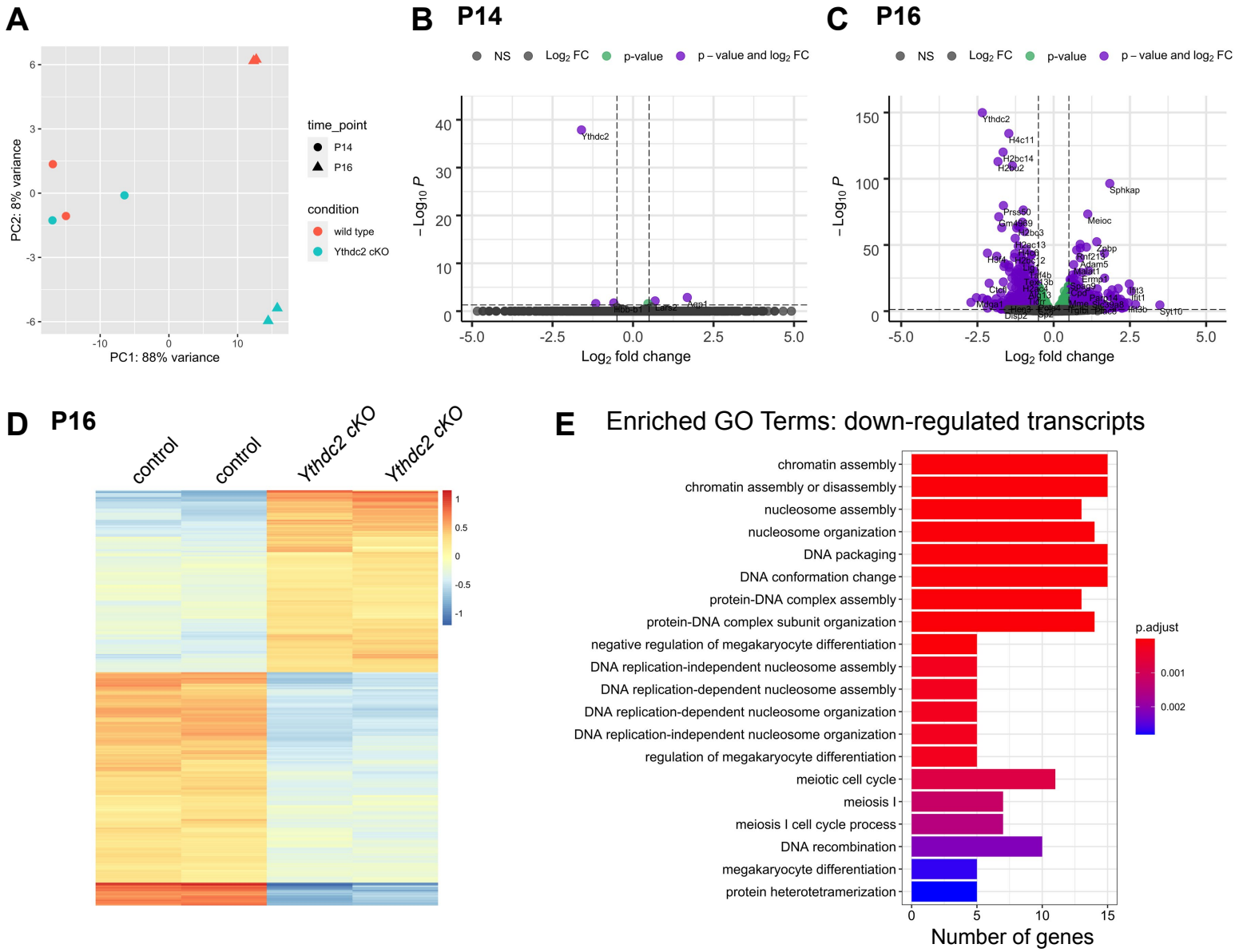
A
PC2: 8% variance
PC1: 88% variance
time_point
P14
P16
condition
wild type
Ythdc2 cKO
B P14
NS
Log2 FC
p-value
p – value and log2 FC
−Log10 P
Log2 fold change
Ythdc2
C P16
NS
Log2 FC
p-value
p – value and log2 FC
−Log10 P
Log2 fold change
Ythdc2
Sphkap
Meioc
D P16
control
control
Ythdc2 cKO
Ythdc2 cKO
E Enriched GO Terms: down-regulated transcripts
chromatin assembly
chromatin assembly or disassembly
nucleosome assembly
nucleosome organization
DNA packaging
DNA conformation change
protein-DNA complex assembly
protein-DNA complex subunit organization
negative regulation of megakaryocyte differentiation
DNA replication-independent nucleosome assembly
DNA replication-dependent nucleosome assembly
DNA replication-dependent nucleosome organization
DNA replication-independent nucleosome organization
regulation of megakaryocyte differentiation
meiotic cell cycle
meiosis I
meiosis I cell cycle process
DNA recombination
megakaryocyte differentiation
protein heterotetramerization
p.adjust
Number of genes

687 **Figure 5. Early transcript changes following knockout of *Ythdc2* in spermatocytes.**

688 (A) Principal component analysis (PCA) of the P14 and P16 control (+/+; *Ythdc2*$^{flox/\Delta}$) and

689 *Ythdc2* cKO (*UBC-CreERT2; Ythdc2*$^{flox/\Delta}$) replicates. Principal component (PC) 1 splits the

690 samples by time point and component 2 splits the samples by genotype. (B, C) Volcano plots

691 representing significantly differentially expressed genes in *Ythdc2* cKO testes relative to control

692 at (B) P14 and (C) P16. Significant differentially expressed genes with cutoffs: Log2FC > 1 or <

693 -1 and p-value < 0.05 are represented in purple, differentially expressed genes with cutoff: p-

694 value < 0.05 are represented in green and non differentially expressed genes are represented in

695 grey. (D) Heatmap representing 294 transcripts differentially expressed in P16 *Ythdc2* cKO

696 testes compared to controls. Biological replicates for both control and *Ythdc2* cKO are shown.

697 Top: 129 transcripts higher in the *Ythdc2* cKO compared to the control (Log2FC > 1, p-value <

698 0.05). Bottom: 165 transcripts down in the *Ythdc2* cKO compared to the control (Log2FC < -1,

699 p-value < 0.05). (E) The top 20 significant Biological Processes GO terms for the genes

700 expressed at lower levels (Log2FC < -1, p-value < 0.05) in P16 *Ythdc2* cKO testes compared to

701 control testes. See also Figure 5 – source data 1.

Table 1. Expression pattern of YTHDC2 protein binding partners in spermatocytes

Protein	Function	Protein expression pattern in spermatocytes by immunofluorescence
MEIOC	Regulation of RNA stability	Leptotene, zytotene and pachytene spermatocytes (cytoplasmic)
PABPC1	Regulation of RNA stability, translation initiation and RNA degradation.	Low in leptotene and zygotene / high in pachytene spermatocytes (cytoplasmic)
FMR1	Regulaton of RNA stability, translation elongation, RNA processing and RNA transport	Leptotene, zygotene and early pachytene spermatocytes (cytoplasmic)
CAPRIN1	Regulation of translation and RNA transport	Pachytene spermatocytes (cytoplasmic)
PTBP1	Regulation of alternative splicing (nucleus) and RNA localization, stability and translation (cytoplasm)	Leptotene and zygotene spermatocytes (cytoplasmic)
EWSR1	Transciption coregulator activity and RNA binding	Leptotene zytotene (cytoplasmic and nuclear), pachytene (nuclear)
MOV10	Regulation of RNA stability, translation, RNA cleavage/gene silencing by miRNA	Leptotene and zygotene spermatocytes (cytoplasmic)
YBX1	Regulation of RNA stability, RNA processing, translational repression and splicing	Pachytene spermatocytes (cytoplasm)
G3BP2	Scaffold protein, granule assembly, RNA transport	Leptotene and zygotene spermatocytes (cytoplasmic)
UPF1	Regulation of nonsense mediated mRNA decay, RNA destabilization	Pachytene spermatocyts (cytoplasmic)

FIGURE SUPPLEMENTS

Figure 1 - figure supplement 1.

A

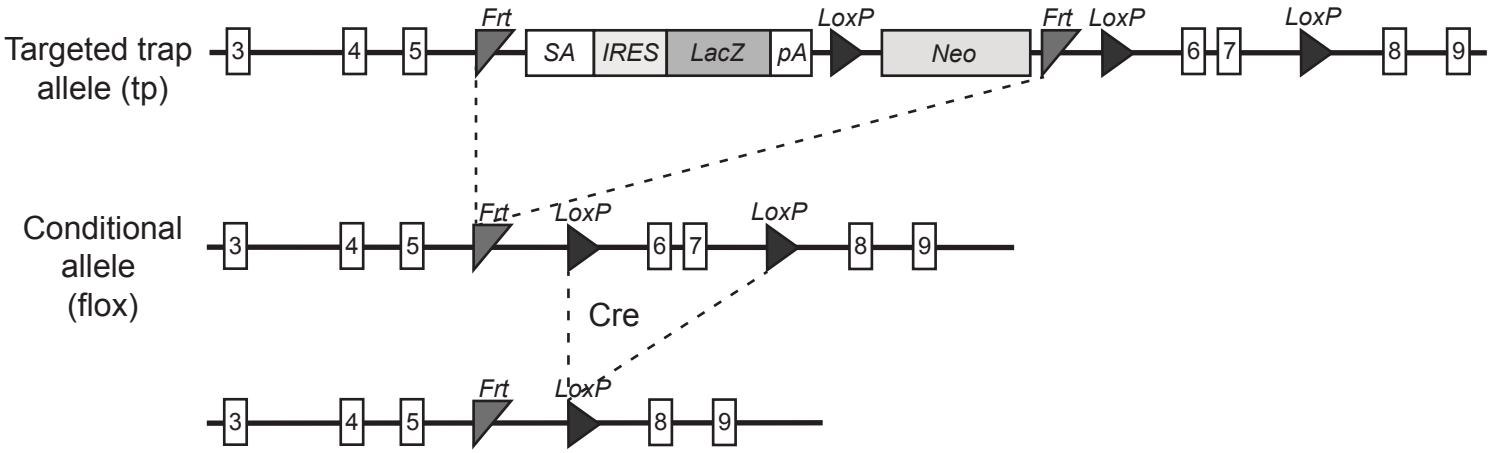

B

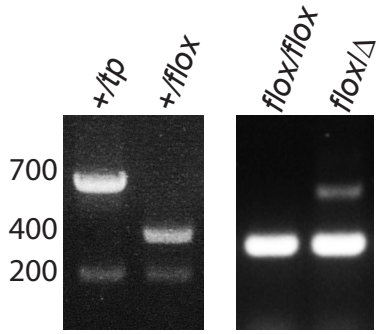

702 **Figure 1 – figure supplement 1. Generation of the *Ythdc2* conditional knockout mouse.**

703 (A) Diagram of the generation of the *Ythdc2* conditional allele (*flox*) from the targeted trap allele

704 (*tp*) through excision of the LacZ reporter and the Neomycin cassette. Cre-mediated deletion of

705 exons 6 and 7 occurs in the *Ythdc2* floxed mice upon exposure to Cre recombinase.

706 SA, splice acceptor; IRES, internal ribosome entry site; LacZ, β-galactosidase gene; pA,

707 polyadenylation sequence; LoxP, Cre recombinase recognition site; FRT, flippase recognition

708 site. (B) Mouse genotyping by PCR analysis of DNA purified from mice heterozygous for the

709 targeted trap allele (*+/tp*), heterozygous for the conditional allele (*+/flox*), homozygous for the

710 conditional allele (*flox/flox*) and heterozygous for the conditional and null allele (*flox/*Δ).

Figure 3 - figure supplement 1.

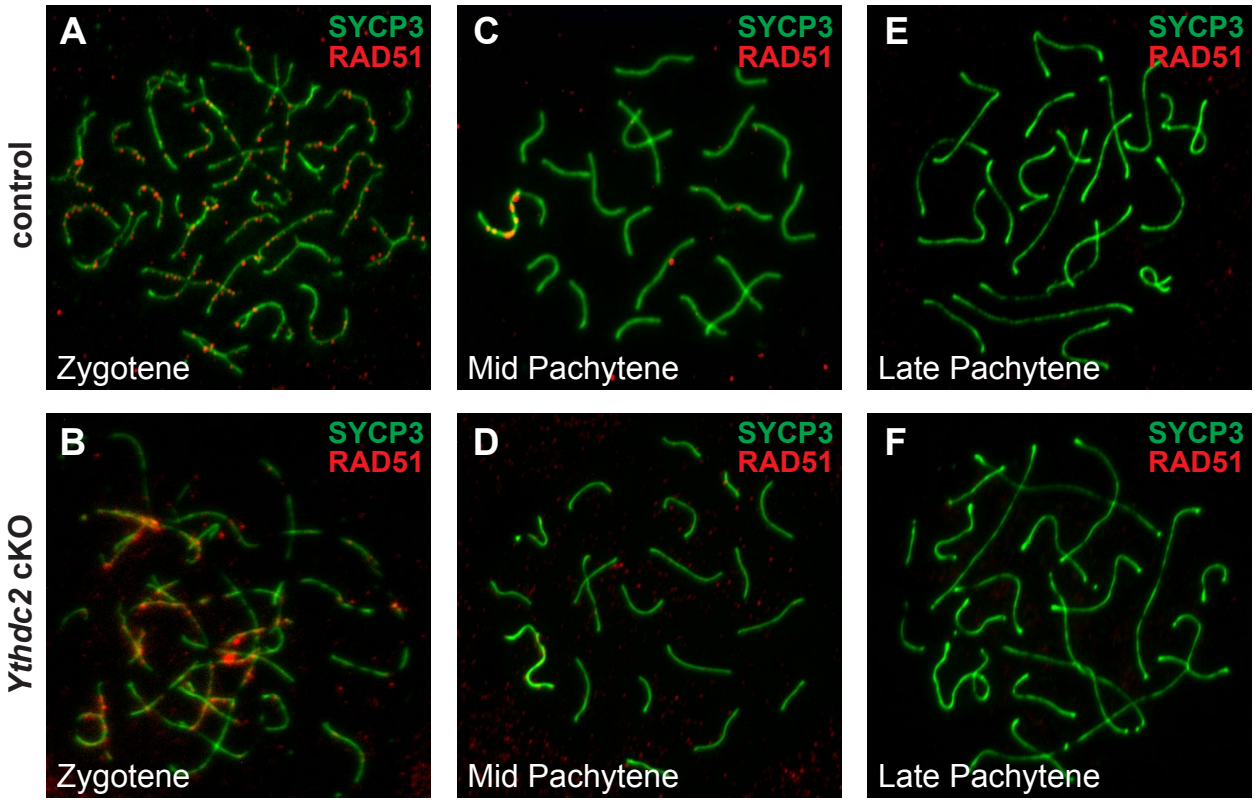

711 **Figure 3 – figure supplement 1. Normal expression pattern of RAD51 in early and late**

712 **spermatocytes.** (A-F) Immunofluorescence images of germ cell spreads from P18 control (+/+*;*

713 *Ythdc2*$^{flox/\Delta}$, top) and *Ythdc2* cKO (*UBC-CreERT2; Ythdc2*$^{flox/\Delta}$, bottom) mice stained for SYCP3

714 (green) and RAD51 (red).

Figure 3 - figure supplement 2.

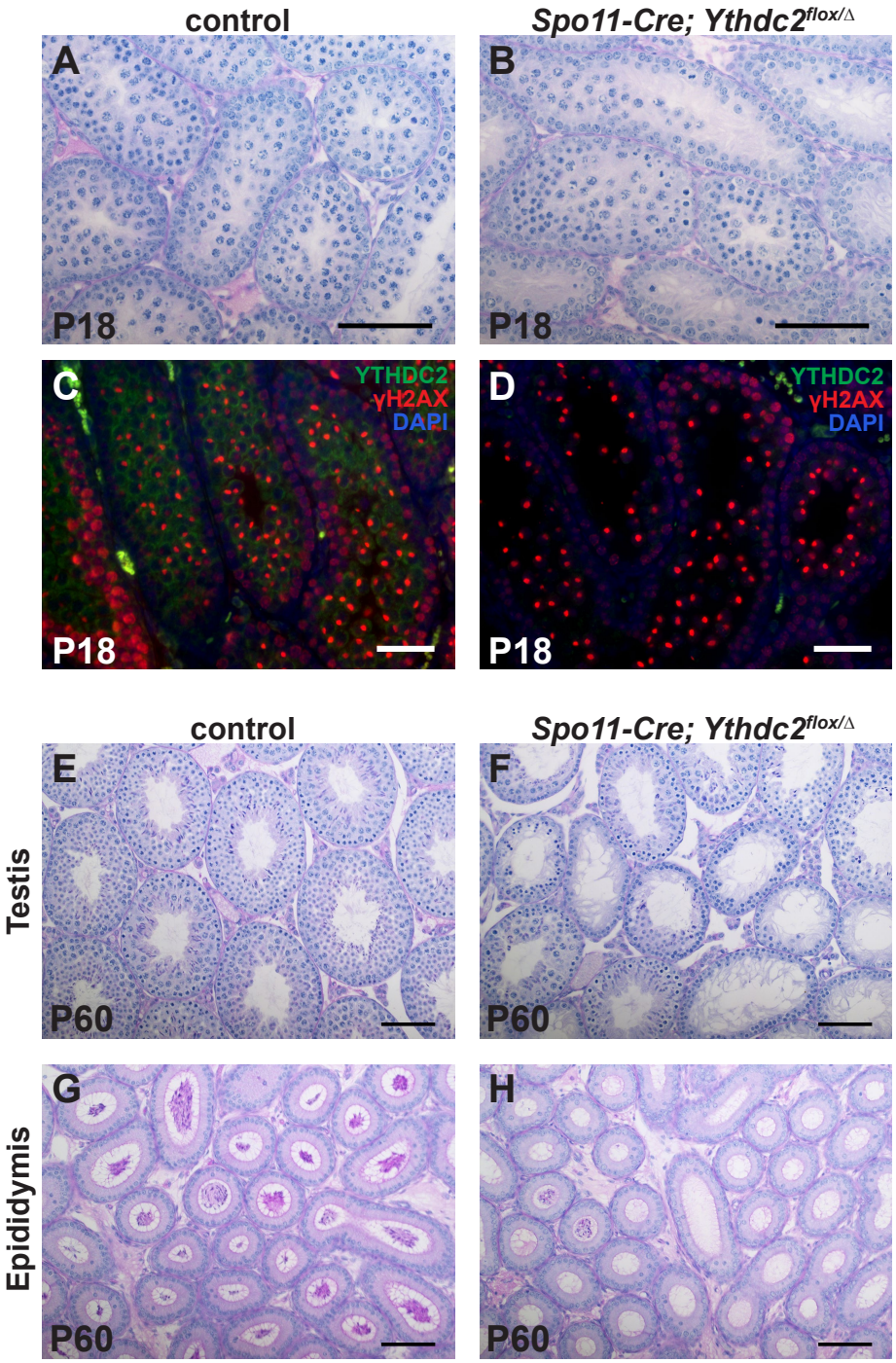

715 **Figure 3 – figure supplement 2. Knocking out *Ythdc2* using the *Spo11-Cre* driver leads to a**
716 **similar phenotype as the inducible driver strategy.** (A, B) Cross-sections of mouse
717 seminiferous tubules stained with periodic acid-Schiff (PAS) from P18 (A) control and (B)
718 *Spo11-Cre; Ythdc2*$^{flox/\Delta}$ mice. (C, D) Immunofluorescence images of P18 (C) control and (D)
719 *Spo11-Cre; Ythdc2*$^{flox/\Delta}$ mouse testis tubule cross-sections stained for YTHDC2 (green), γH2AX
720 (red) and DAPI (blue). (E, F) Cross-sections of mouse seminiferous tubules stained with periodic
721 acid-Schiff (PAS) from P60 (E) control and (F) *Spo11-Cre; Ythdc2*$^{flox/\Delta}$ mice. (G, H) Cross-
722 sections of mouse epididymis stained with periodic acid-Schiff (PAS) from P60 (G) control and
723 (H) *Spo11-Cre; Ythdc2*$^{flox/\Delta}$ mice. Scale bars: 50 μm.

724 **LIST OF FIGURE SUPPLEMENTS AND SOURCE DATA FILES:**

725 **Figure 1 – figure supplement 1.** Generation of the *Ythdc2* conditional knockout mouse.

726 **Figure 3 – figure supplement 1**. Normal expression pattern of RAD51 in early and late

727 spermatocytes.

728 **Figure 3 – figure supplement 2.** Knocking out *Ythdc2* using the *Spo11-Cre* driver leads to a

729 similar phenotype as the inducible driver strategy.

730 **Figure 4 - source data 1.** Original files for western blots in Figure 4A.

731 **Figure 4 - source data 2.** Original files for western blots in Figure 4B.

732 **Figure 5 - source data 1.** Differentially expressed genes in P16 *Ythdc2* cKO compared to

733 control testes.